Optica Applicata, Vol. XXIX, No. 4, 1999

Scattering of light by objects of atmospheric particle size

KRYSTYNA KOLWAS, MACIEJ KOLWAS

Institute of Physics of the Polish Academy of Sciences, al. Lotników 32/46, 02–668 Warszawa, Poland.

We study the scattering, absorption and extinction properties of particles of atmospheric size (from few nanometers to 1 micron) on the basis of several pertinent examples. The description is based on the Mie scattering theory. As an illustration we recall the laboratory experiment on scattering properties of sodium droplets induced by light.

1. Introduction

In atmospheric air there is an enormous amout of particulate matter of different size, shape and origin. Some of these constituents are classified as pollutants, because they can be (or they are) above certain concentration harmful to life and materials. Beside gas pollutants there are particles transported by the air flow in an amount estimated at 1000 to 2500 billion kilograms per year [1]. Particles can be introduced into the atmosphere from natural sources (*e.g.*, wind-blown dust or aerosols of different kind, particles of sea salt from ocean), or can be created by human activity through combustion, abrasion of machinery, industrial and agricultural processes. Their sizes range from 10^{-2} μm to 100 μm in diameter. There are several methods of sampling single particles, which rely, *e.g.*, on mass-spectroscopy or chemical analysis. There are also some optical methods (*e.g.*, [2]–[4]) relying on scattering properties of particles. In the paper, we illustrate some scattering properties of chosen particles of atmospheric size.

The scattering abilities of an object depend on its size, shape and on material properties described, *e.g.*, by the complex index of refraction. The optical diagnostic methods allow us to some extent to learn about the type of particles. Investigation of some unknown particles relies on the comparison of measured optical signals with theoretical predictions by assuming the size and shape of a particle and its material properties. The success of fitting the predicted signals (with some parameters let free) to those obtained from experiments is the basis for diagnosis.

The most useful theoretical approach to the problem of diffraction of light by a spherical particle of any size was developed almost one hundred years ago by Mie [5]. In the Mie theory, the interaction of a particle with light of a given wavelength is treated by solving Maxwell's equations with boundary conditions at the spherical surface, across which the properties of the medium change abruptly. In spherical polar coordinates the light field is represented as a sum of two modes (two

"subfields"), one with nonzero radial component of the electric field (transverse-magnetic mode – TM mode), and the second one, with no radial component of the electric field (transverse-electric mode – TE mode). The scattered and the absorbed fields, which are the solution of the problem, are represented as an infinite series for both modes. The Mie scattering theory for a sphere is an analogue of Fresnel scattering formulas for planar surface.

We illustrate below the prediction of the Mie theory for some spherical particles as a function of their radii within the size range corresponding to the size of atmospheric particles. We show how different observables are sensitive to the index of refraction of matter forming a particle. We use at least the first 50 terms of the series of the Mie solutions in both modes. According to the criterion $\frac{2\pi R}{\lambda} \ll l = 50$ (R is the particle radius, λ is the wavelength of the light field), this approximation is correct for particle radii up to $R \approx 1$ μm when using the visible light ($\lambda \simeq 0.5$ μm). This size range covers well the smallest and medium sized aerosol particles and enables the study of the dependence of optical properties of a single particle on its radius for different material properties of an object. We also shortly discuss the properties of sodium droplets produced and studied optically in the laboratory as a function of their size. We compare our experimental data with predictions of the Mie theory.

2. Scattering, extinction and absorption (Mie scattering theory)

One of the observables described by the Mie theory is the intensity of light scattered at a given angle with respect to the direction of the incoming light. For linear polarization of the incident light, the scattered light is, in general elliptically polarized. However, when the plane of observation is parallel or perpendicular to the polarization direction of the incident light (see Fig. 1), the scattered light is expected to be linearly polarized, with intensities depending on the direction of observation.

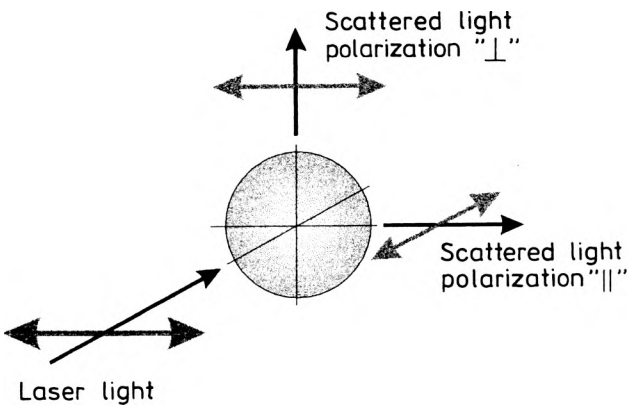

Fig. 1. Geometry of observation of scattered light for measuring $I_{\parallel}$ or $I_{\perp}$ intensities ((Eqs. (1), (2)) for $\Theta = \pi/2$.

This particular situation defines the two orthogonal geometries of the experiment, resulting in different dependence of the scattered intensities $I_{\parallel}(R)$ or $I_{\perp}(R)$ on particle size. The measured intensities depend on whether we observe the light in the plane containing the the direction of polarization and the direction of the incident beam (parallel polarization $\parallel$) or whether we observe the light perpendicular to this direction (perpendicular polarization $\perp$), [5] (see Fig. 1):

$$I_{\parallel}(R) = I_0\left[\frac{\lambda}{2\pi r}\left|\sum_{l=1}^{\infty}(-i)^l\left({}^{\mathrm{TE}}B_l(R)P_l^{(1)'}(\cos\Theta)\sin\Theta - {}^{\mathrm{TM}}B_l(R)\frac{P_l^{(1)}(\cos\Theta)}{\sin\Theta}\right)\right|\right]^2, \quad (1)$$

$$I_{\perp}(R) = I_0\left[\frac{\lambda}{2\pi r}\left|\sum_{l=1}^{\infty}(-i)^l\left({}^{\mathrm{TE}}B_l(R)\frac{P_l^{(1)}(\cos\Theta)}{\sin\Theta} - {}^{\mathrm{TM}}B_l(R)P_l^{(1)'}(\cos\Theta)(\sin\Theta)\right)\right|\right]^2 \quad (2)$$

where: I_0 is the intensity of incoming field, r is the distance from the scattering object, Θ is the angle between directions of propagation and observation,

$${}^{\mathrm{TE}}B_l(R) = i^{l+1}\frac{2l+1}{l(l+1)}\frac{\sqrt{\varepsilon_{\mathrm{in}}}\psi_l'(\rho\sqrt{\varepsilon_{\mathrm{out}}})\psi_l(\rho\sqrt{\varepsilon_{\mathrm{in}}}) - \sqrt{\varepsilon_{\mathrm{out}}}\psi_l(\rho\sqrt{\varepsilon_{\mathrm{out}}})\psi_l'(\rho\sqrt{\varepsilon_{\mathrm{in}}})}{\sqrt{\varepsilon_{\mathrm{in}}}\xi_l'(\rho\sqrt{\varepsilon_{\mathrm{out}}})\psi_l(\rho\sqrt{\varepsilon_{\mathrm{in}}}) - \sqrt{\varepsilon_{\mathrm{out}}}\xi_l(\rho\sqrt{\varepsilon_{\mathrm{out}}})\psi_l'(\rho\sqrt{\varepsilon_{\mathrm{in}}})}, \quad (3)$$

$${}^{\mathrm{TM}}B_l(R) = i^{l+1}\frac{2l+1}{l(l+1)}\frac{\sqrt{\varepsilon_{\mathrm{in}}}\psi_l(\rho\sqrt{\varepsilon_{\mathrm{out}}})\psi_l'(\rho\sqrt{\varepsilon_{\mathrm{in}}}) - \sqrt{\varepsilon_{\mathrm{out}}}\psi_l'(\rho\sqrt{\varepsilon_{\mathrm{out}}})\psi_l(\rho\sqrt{\varepsilon_{\mathrm{in}}})}{\sqrt{\varepsilon_{\mathrm{in}}}\xi_l(\rho\sqrt{\varepsilon_{\mathrm{out}}})\psi_l'(\rho\sqrt{\varepsilon_{\mathrm{in}}}) - \sqrt{\varepsilon_{\mathrm{out}}}\xi_l'(\rho\sqrt{\varepsilon_{\mathrm{out}}})\psi_l(\rho\sqrt{\varepsilon_{\mathrm{in}}})}, \quad (4)$$

$P_l^{(1)}(z)$ are th l-the order Legendre polynomials of the first kind:

$$P_l^{(1)}(\cos\Theta) = \frac{l}{\sin\Theta}(P_{l-1}(\cos\Theta) - \cos\Theta P_l(\cos\Theta)) \quad (5)$$

where

$$P_l(\cos\Theta) = \sum_{m=0}^{\mathrm{floor}(l/2)}(-1)^m\frac{(2l-2m)!}{2^l m!(l-m)!(l-2m)!}\cos\Theta)^{l-2m}, \quad (6)$$

and $P_l^{(1)'}(z)$ is the derivative with respect to the argument of l-th order Legendre polynomials:

$$\frac{dP_l^{(1)}(\cos\Theta)}{d(\cos\Theta)} = \frac{(l+1)P_{l-1}^{(1)}(\cos\Theta) - l\cos\Theta P_l^{(1)}(\cos\Theta)}{\sin\Theta}, \quad (7)$$

$\rho = 2\pi R/\lambda$, $\psi_l(x) = \sqrt{\frac{\pi x}{2}}J_{l+1/2}(x)$ and $\xi_l(x) = \sqrt{\frac{\pi x}{2}}H_{l+1/2}^{(1)}(x) = \sqrt{\frac{\pi x}{2}}J_{l+1/2}(x) - iN_{l+1/2}(x))$. $J_{l+1/2}(x)$, $H_{l+1/2}^{(1)}(x)$ and $N_{l+1/2}(x)$ are Bessel, Hankel and Neuman cylindrical functions with the arguments $\rho\sqrt{\varepsilon_{\mathrm{out}}}$ and $\rho\sqrt{\varepsilon_{\mathrm{in}}}$, respectively. $\varepsilon_{\mathrm{in}}$ and $\varepsilon_{\mathrm{out}}$ are the dielectric functions of the particle and of the surroundings, respectively. Below, all the particles studied are assumed to be suspended in a medium optically resembling vacuum, $\varepsilon_{\mathrm{out}} = 1$. The complex, relative index of refraction is then defined as $m = \sqrt{\varepsilon_{\mathrm{in}}}$. The superscripts TM and TE denote transverse magnetic and transverse electric modes of the field.

A measure of the scattering properties of a sphere as a whole is the total scattering cross-section, given by the ratio of flow of the total scattered energy to the energy density of the incident wave [6]

$$\sigma_{\text{scat}}(R) = \frac{\lambda}{2\pi}\left[\sum_{l=1}^{\infty}(-i)^{l+1}l(l+1)(|^{\text{TE}}B_l(R)|^2+|^{\text{TM}}B_l(R)|^2)\right], \tag{8}$$

while the sum of the total absorbed and scattered energy flow defines the extinction cross-section

$$\sigma_{\text{ext}}(R) = \frac{\lambda}{2\pi}\text{Re}\left[\sum_{l=1}^{\infty}(-i)^{l+1}l(l+1)(^{\text{TE}}B_l(R)+{}^{\text{TM}}B_l(R))\right]. \tag{9}$$

The resulting total absorption cross-section of a sphere is then

$$\sigma_{\text{abs}} = \sigma_{\text{ext}} - \sigma_{\text{scat}}. \tag{10}$$

All these observables are quickly growing functions of particle size changing in character and depending on how large the particle is in comparison with the light wavelength. To study this dependence it is convenient to introduce some optical quantities, which correspond not to a single particle, but to the unit surface of a single particle [7]. The corresponding quantities define the efficiency of scattering, extinction and absorption per unit surface, respectively: $\sigma_{\text{scat}}(R)/\pi R^2$, $\sigma_{\text{ext}}(R)/\pi R^2$, $\sigma_{\text{abs}}(R)/\pi R^2$.

For particles smaller than the wavelength ($2\pi R/\lambda \ll 1$) the quasi-static approximation is valid: in that case the electric field does not change within the particle, and the resulting static polarizability does not depend on the light wavelength. The scattering by a particle with size within this region corresponds to the so-called Rayleigh scattering; the particle scatters the light as a radiating dipole in an external electromagnetic field. For Rayleigh scattering, the total scattering cross-section is proportional to $\lambda^4 R^6$, while the total absorption cross-section is proportional to R^3/λ [8]. A graphic illustration of the scattering, absorption and extinction properties in the form of efficiencies per unit surface $\sigma_{\text{scat}}(R)/\pi R^2$, $\sigma_{\text{ext}}(R)/\pi R^2$, $\sigma_{\text{abs}}(R)/\pi R^2$ is convenient and allows us to distinguish easily the region of particle sizes, for which a particle scatters the light as a Rayleigh particle. The absorption efficiency $\sigma_{\text{abs}}(R)/\pi R^2$ is a linear function of the radius R and in the corresponding region of sizes the scattering efficiency $\sigma_{\text{sca}}(R)/\pi R^2$ is proportional to R^4.

3. Water particle

An an example let us consider the water droplets with size changing up to 1000 nm. Figure 2 presents the extinction, absorption and scattering efficiencies as a function of the particle size for different light wavelengths.

According to Figure 2**a**, the water droplet, when illuminated by infrared light ($\lambda = 10$ μm), behaves like a small particle. It absorbs and scatters the electromagnetic field as a Rayleigh particle: the absorption efficiency is a linear function of the particle size, the corresponding absorption cross-section is proportional to R^3, *i.e.*, the volume

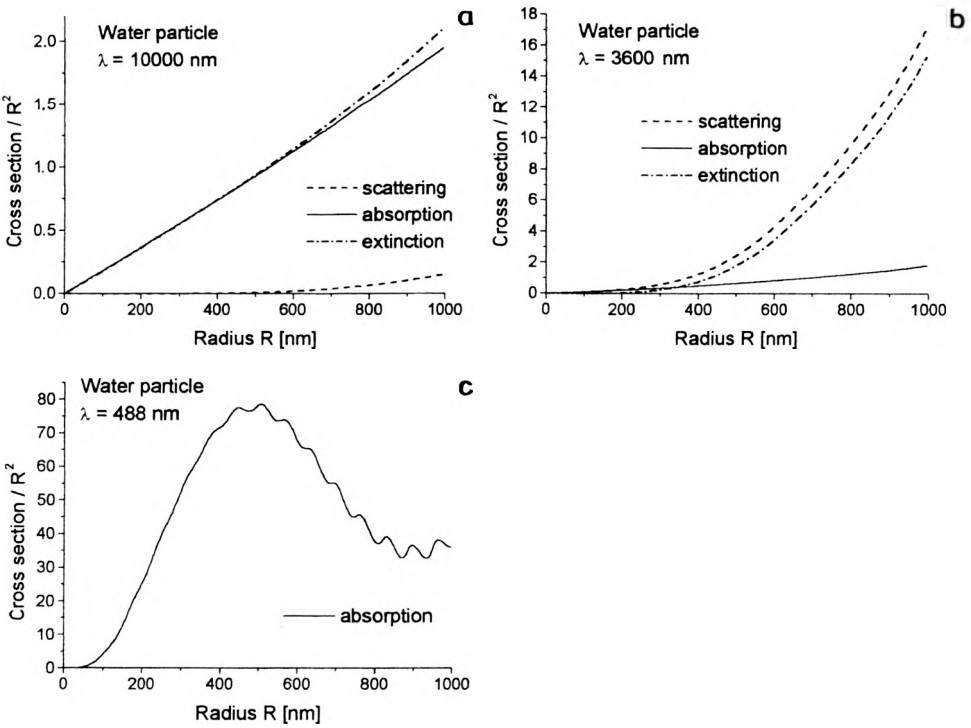

Fig. 2. Extinction, scattering and absorption efficiencies of a water droplet as a function of particle size: **a** — in infrared ($\lambda = 10$ μm, $m = 1.22 + i0.06$, **b** — in near infrared ($\lambda = 3.6$ μm, $m = 1.42 + i0.014$), **c** — in visible light (no absorption, scattering equals extinction; $\lambda = 488$ nm, $m = 1.33$).

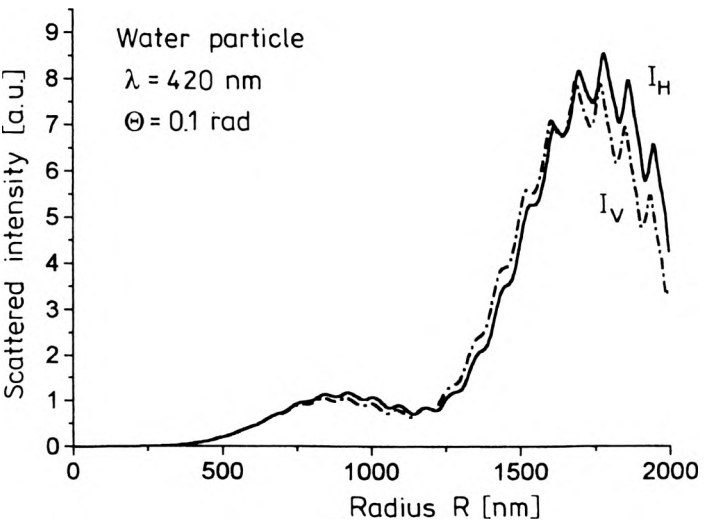

Fig. 3. Intensities $I_{\parallel}(R)$ and $I_{\perp}(R)$ scattered at small angle ($\Theta = 0.1$ radian) with respect to the incoming light ($\lambda = 420$ nm).

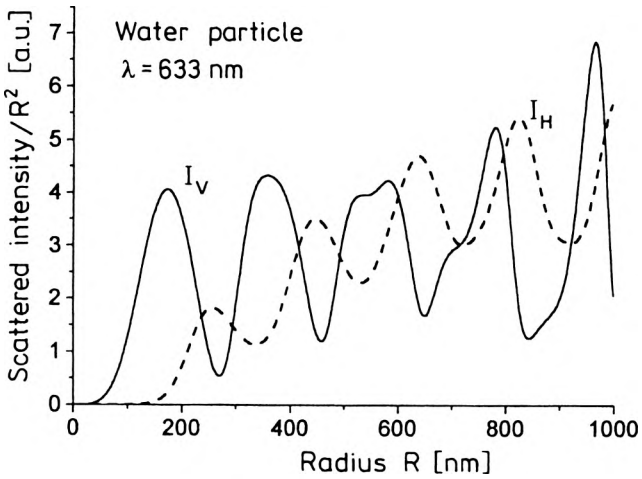

Fig. 4. Intensities $I_{\parallel}(R)$ and $I_{\perp}(R)$ scattered at right angle ($\Theta = 90°$) with respect to the incoming light ($\lambda = 630$ nm).

of the particle. In the infrared radiation the main process is the absorption (heating of a droplet), which dominates the particle extinction.

In near infrared ($\lambda = 3.6$ μm), see Fig. 2**b**, the water drop becomes a partially transparent object. The absorption evolves into a less dominant process than the scattering for a droplet with radii exceeding 400 nm. In the near infrared, the particle is again seen as a Rayleigh particle: the absorbing efficiency is an almost linear function of size, and scattering efficiency depends on size almost as R^4.

In the visible blue light ($\lambda = 488$ nm), the same particles are completely transparent (no noticeable absorption) and the extinction cross-section is equivalent to the scattering cross-section (see Fig. 2**c**). A drop with a size of a few nanometers is seen as a large particle in that light. For most sizes in the region studied, the electromagnetic field intensity changes within the particle and the quasi-static approximation $2\pi R/\lambda \ll 1$ is not fulfilled. The scattering cross-sections show two kinds of behaviour: slow oscillations due to the interference of TM and TE contributions of l-th orders, and the ripple structure due to the so-called morphology dependent resonances, corresponding to the multiple scattering of light inside the drop [8].

A similar rich structure can also be seen when observing the intensity of light scattered at a small angle with respect to the direction of incidence (Fig. 3). In that case the two polarization intensities $I_{\parallel}(R)$ and $I_{\perp}(R)$ are almost equal functions of droplet size. However, when observing the scattered light at right angles (Fig. 4), there is no ripple structure — only "interference" oscillations are present. As seen in Fig. 4, the visibility of a particle with a given size depends strongly on the observation geometry. The droplets with size corresponding to $R \approx 160$ nm, 340 nm, 500 nm, and so on, are seen as a bright object when observed in $\perp$ geometry, while in $\parallel$ geometry, droplets with the same size are hardly seen.

The analysis of Figures 2—4 shows that the optical response of a droplet can be very sensitive to its size, the light wavelength and direction of observation.

4. Examples of optical properties of particles with specific index of refraction

As examples of non-transparent particles we have chosen particles built up from matter with low and high values of a real and an imaginary part of the complex index of refraction: a particle of carbon ($m = 0.59 + i0.66$) and a particle of sodium ($m = 0.186 + i1.592$), [8].

Figure 5**a** illustrates efficiencies of absorption, scattering and extinction, which show smooth dependence on particle size. The Rayleigh type of scattering by the oscillating electric dipole is responsible for the initial growth of scattering and

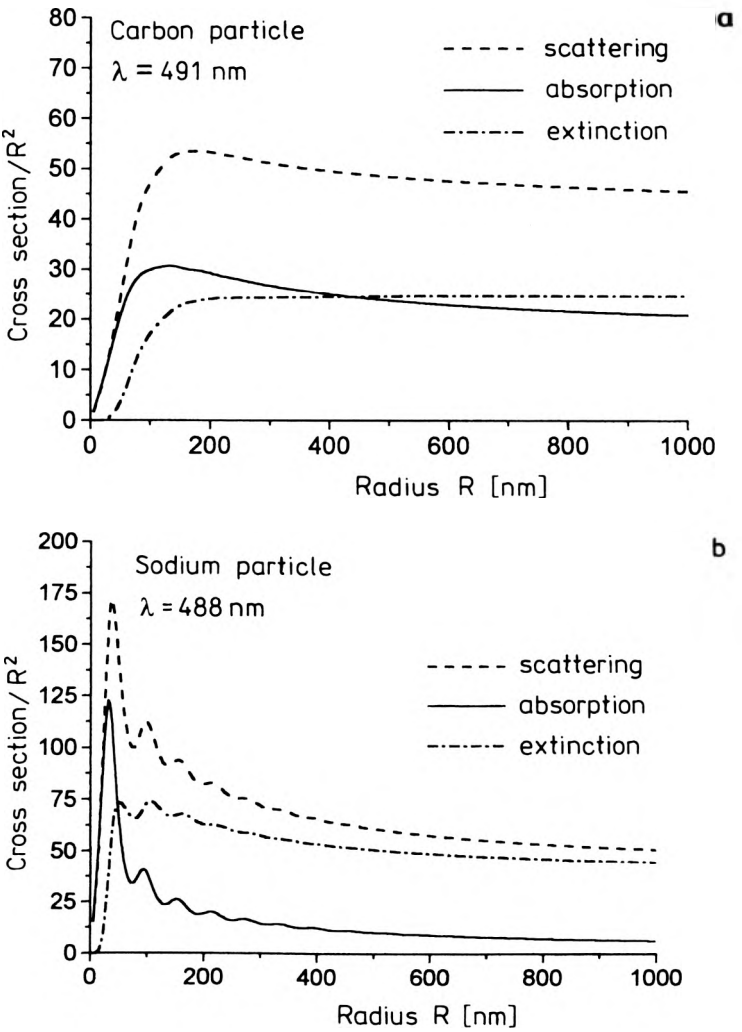

Fig. 5. Extinction, scattering and absorption efficiencies as a function of particle size in visible light for: **a** — carbon particle ($m = 1.59 + i0.66$), **b** — sodium particle ($m = 0.186 + i1.592$).

absorption efficiencies. This region of particle sizes is visible in Fig. 5a as a linear growth of absorption efficiency and the corresponding growth of scattering proportional to $\sim R^4$ for particle range up to about $R = 80$ nm. The further weak dependence of the scattering efficiency shows that the total scattering cross-section becomes, to a good approximation, the quadratic function of the particle size.

Contrary to carbon, the sodium particle within the same size range shows some characteristic maxima in the dependence of its absorption, scattering and extinction efficiencies on particle radius (see Fig. 5b). Sodium is the best representative of

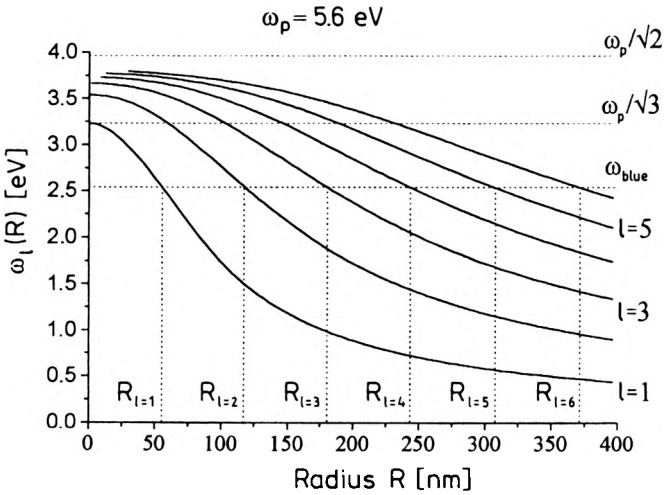

Fig. 6. Resonance frequencies of plasmon oscillations as a function of the radius of sodium particle. $l = 1$ corresponds to the dipole plasmon, $l = 2$ corresponds to the quadrupole plasmon, while higher order l corresponds to the higher order multipolarity plasmon excitations [7].

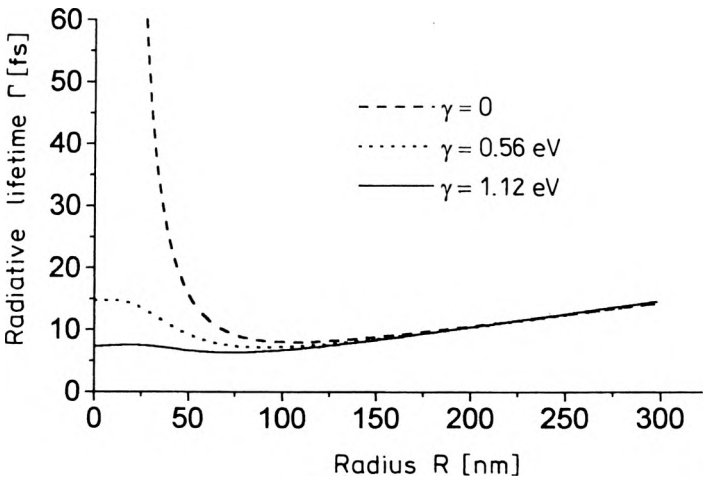

Fig. 7. Radiative decay of dipole plasmon oscillations in a sodium droplet for different relaxation rates γ of the free-electron plasma.

free-electron metals and its optical characteristics results directly from the properties of free-electron gas filling the particle. In [7], we have shown that the maxima appearing in the scattering efficiency for given particle sizes result from the contributions to the scattering of the secondary fields due to the excitation of collective electron oscillations (plasmons). The model is based on the fact that a sphere filled with free-electron gas forms a cavity with size dependent eigenfrequencies of the optically excitable TM surface plasmons. The real part of the eigenfrequency $\omega_l(R)$, $l = 1, 2, 3 \ldots$, (Fig. 6) defines the frequency of the light field, enabling the resonant excitation of a plasmon oscillation in a cluster with appropriate size, while the imaginary part of the eigenfrequency defines the radiative decay rate $1/\Gamma_l(R)$ of the excited plasmon oscillations. The Drude dielectric function of the free-electron gas was used to describe the optical properties of the material forming the sodium droplet. Both quantities: the resonant frequency $\omega_l(R)$ and the radiative decay rate $1/\Gamma_l(R)$ are modified by the relaxation rate γ of the free-electron gas entering the Drude dielectric function. However, the modification of the resonance frequency is weak [7], contrary to the meaningful modification of the radiative decay time Γ_l of the plasmon oscillations. Figure 7 illustrates radiative decay time $\Gamma_l(R)$ of the dipole plasmon oscillations for different values of the assumed damping rates γ of free-electron plasma [9].

In the next chapter, we will recall some results of the laboratory experiment on scattering properties of sodium droplets, which were optically induced from the vapour phase.

5. Experimental study of scattering properties of sodium droplets

Presently available data on photoabsorption cross-sections of metal particles concern mainly mass-selected microclusters consisting of a few up to several tens of atoms in a particle [10]–[14]. Peaks appearing in the spectra were usually assigned to the expected position of the Mie resonance. Most optical experiments on free large metal clusters have been performed in dusty or aerosol media [15]–[19]. Experiments on very large free metal clusters of the size of the order of 100 nm or larger and with narrow size distribution are not so common [9], [20]–[23].

In papers [20], [21], we have proposed a new method of large cluster formation, *i.e.*, of particles with size as large as hundreds of nanometers. The process is initiated by laser light passing through the sample consisting of saturated vapour of sodium atoms, sodium dimers (two-atom particles) and helium buffer gas under high, almost atmospheric pressure. The switching-on of the laser light, which is resonant to the dimer transition (488 nm line of the argon-ion laser) produces supersaturation of the sodium vapour. Some dimer molecules resonantly excited by light, experience dissociation assisted by collisions with buffer gas atoms. The atoms arising from dissociated dimers give an excess of atoms in previously saturated sodium vapour. The resulting supersaturation enables condensation of clusters. The process develops with time and lasts from a few up to a few tens of seconds [22]. The dynamics of the

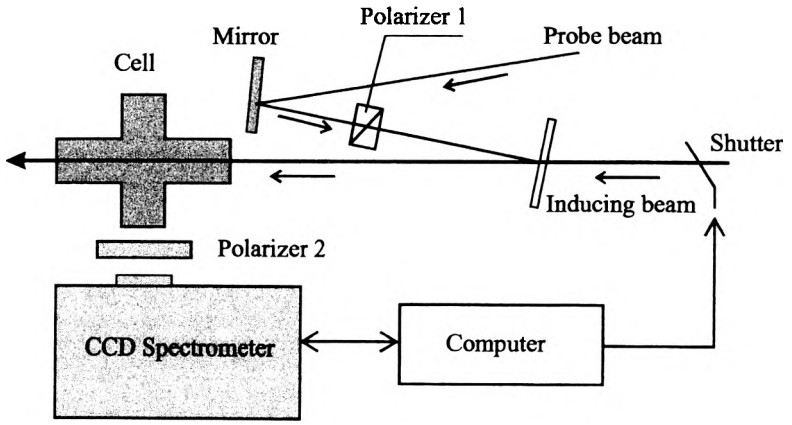

Fig. 8. Scheme of the experimental set-up for the production of sodium droplets by light.

process depends on experimental conditions defined by the temperature of the oven, the pressure of the helium gas, and the intensity of the laser light. We can observe a smooth change of optical properties of clusters which grow from an atomic microparticle up to a macroscopic droplet of the order of 150 nm.

The experimental scheme is sketched in Fig. 8. The probe beam of the argon-krypton laser is linearly polarized at 45 degrees with respect to the observation plane, defined by the direction of the probe beam and the chosen direction of observation. We measure intensities of the probe light beam scattered at right angle in two polarization geometries [25]: the polarization of the incident and of the detected beam perpendicular to the plane of observation (polarization V corresponding to $\perp$ polarization geometry for a spherical particle), and the polarization of the incident and of the detected beams parallel to the plane of observation (polarization H corresponding to $\parallel$ polarization geometry for the spherical particles), see Figs. 1 and 9. These two orthogonal polarization directions

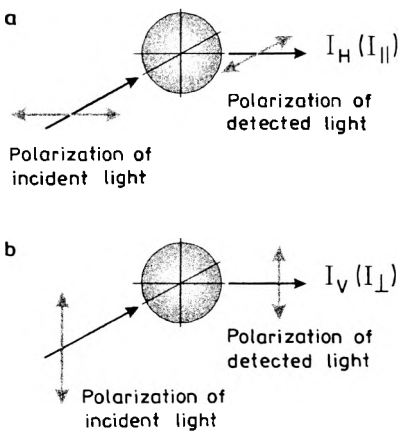

Fig. 9. Two orthogonal polarization geometries for observation of scattered light by light induced sodium droplets.

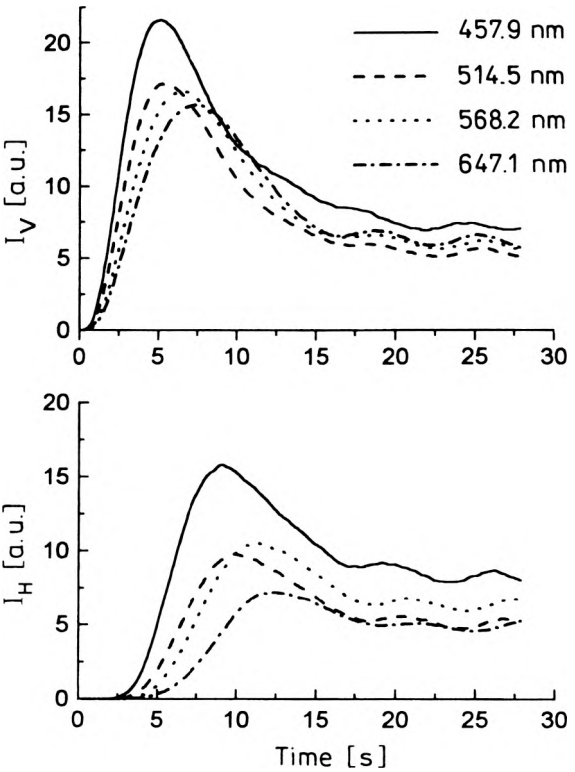

Fig. 10. Measured intensities of light scattered by growing sodium droplets as a function of time for different of wavelengths [24].

of the incident and observed probe beams are selected by the linear polarizers 1 and 2. The measurement of intensities $I_H(t)$ and $I_V(t)$ is repeated for several wavelengths of the probe light beam scattered by growing clusters. An exmple of experimental data [24] is shown in Fig. 10. The zero time corresponds to the switching-on of the laser light initiating cluster production. The experimental signals are taken at a temperature of 500 °C, a helium pressure of 550 torr, Ar^+ laser power of 150 mW, and probe laser power of 10 mW.

Both $I_V(t)$ and $I_H(t)$ at a given wavelength show maxima, however, the maximum in $I_V(t)$ appears earlier (for smaller clusters) than the maximum observed in $I_H(t)$. Both signals stabilize due to cluster size and concentration stabilization. For the given polarization geometry (H or V) the longer the wavelength, the larger the radius corresponding to the maximum of the scattered signal.

We elaborated the method for finding the dependence of the radius and of the concentration of light induced sodium droplets as they grow spontaneously to the final size. The analysis [24] involves experimental study of the scattering of light at different wavelenghts and its comparison with the corresponding expressions $I_{\parallel}(R)$ and $I_{\perp}(R)$ as functions of the size (see Fig. 11), resulting from the Mie scattering theory. The optical properties of sodium droplets under study are described by the

dielectric function of a free-electron plasma. The elaborated algorithm [24] allows the size and the concentration of clusters to be determined at successive stages of droplet growth. Under typical experimental conditions cluster size grows almost linearly with time before reaching the stable size of about 130–150 nm.

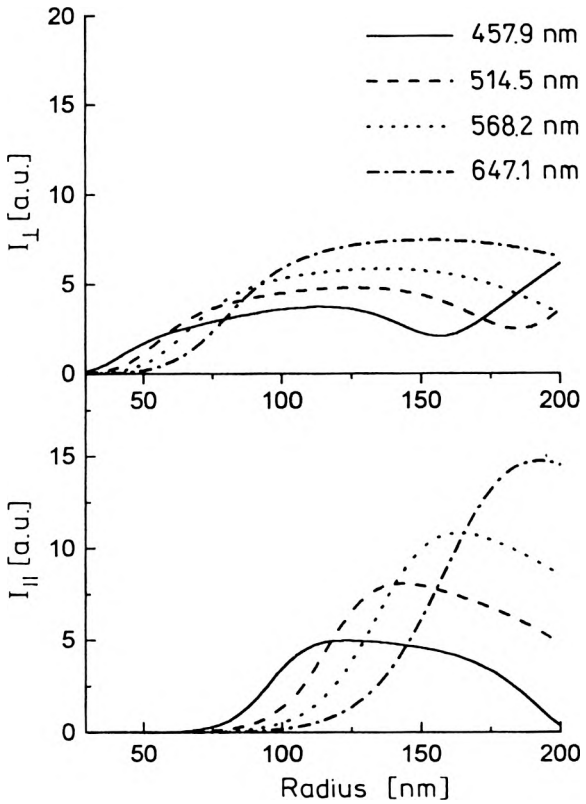

Fig. 11. Scattered light intensities $I_\parallel(R)$ and $I_\perp(R)$ by growing sodium droplets resulting from Mie theory.

To interpret the maxima appearing in measured intensities $I_V(t)$ and $I_H(t)$, we used again the concept of collective electron oscillations excited by light. In paper [25], we have shown that it is the TM mode only which is responsible for maxima appearing in unit surface normalized intensities $I_\parallel(R)/\pi R^2$ and $I_\perp(R)/\pi R^2$ (see Fig. 12), in spite of the fact that for a spherical geometry of a droplet both the TM and the TE contributions are present at every order of l. The TM mode with $l = 1$ is responsible for the maximum in $I_\perp(R)/\pi R^2$, while the maximum in $I_\parallel(R)/\pi R^2$ is due to the TM mode contribution in second order ($l = 2$). We attributed maxima in normalized intensities scattered by a single cluster to the contribution due to resonant excitation of the dipole and quadrupole plasmon, respectively; the maximum in $I_\perp(R)/\pi R^2$ to the dipole surface plasmon, while the maximum in $I_\parallel(R)/\pi R^2$ to quadrupole plasmon [25]. As expected from solving the eigenproblem for the sodium sphere (see Fig. 6), smaller the frequency (the longer the

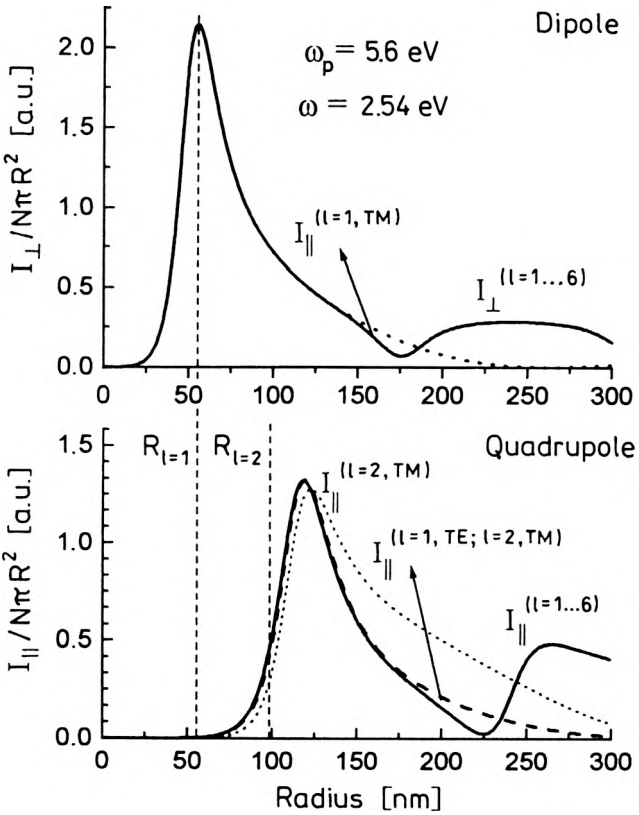

Fig. 12. Normalized intensities $I_{\parallel}(R)/R^2$ and $I_{\perp}(R)/R^2$ [25], illustrating the role of dipole plasmon contribution to $I_{\perp}(R)/R^2$ and of the quadrupole plasmon contribution to $I_{\parallel}(R)/R^2$ scattering.

wavelength) of the light field, the bigger the cluster enabling the resonant excitation of a plasmon with a given multipolarity [7].

The study of dynamics of the cluster growth resulting in finding temporal dependence of size $R(t)$ and concentration $N(t)$ of sodium droplets, allows us to find the experimental intensities of light scattered by the unit surface of a single cluster [24]: $I_V(R(t))/N(t)R^2(t)$ and $I_H(R(t))/N(t)R^2(t)$. These observables correspond to the quantities $I_{\parallel}(R)/R^2$ and $I_{\perp}(R)/R^2$. As expected from the plasmon model, the maxima appearing to $I_V(R(t))/N(t)R^2(t)$ and $I_H(R(t))/N(t)R^2(t)$ dependences show the shift towards larger sizes, when induced by light with larger wavelength. We interpret those maxima as a manifestation of the dipole and the quadrupole plasmon. As far as we know, these data are the only experimental data illustrating the dependence of the plasmon resonance frequency on cluster size in the range of a few tens up to a few hundreds nanometers. The slope of the dependence of plasmon position on the inverse cluster radius [26] is opposite to that derived from the available data on photoabsorption cross-sections in very small mass-selected sodium clusters consisting of a few up to several tens of atoms [27]–[29], see also [26].

Acknowledgements – This work was partially supported by the Polish State Committee for Scientific Research (KBN), grant No. 2 PO3B 016 13.

References

[1] NOBLE CH., PRATHER K., Phys. World **11** (1998), 40.
[2] MEASURES R. M., *Laser Remote Sensing – Fundamentals and Applications*, Krieger Publ. Co., Malabar, Florida, 1992.
[3] CHUDZYŃSKI S., ERNST K., STACEWICZ T., SZYMAŃSKI A., Proc. SPIE **3188** (1997), 168. *Ibidem* p. 180.
[4] FREJAFON E., KASPARIAN J., RAMBALDI P., VEZIN B., BOUTOU V., YU J., ULBRICHT M., WEIDAUER D., OTTOBRINI B., DE SAEGER E., KRAMER B., LEISNER T., RAIROUX P., WÖSTE L., WOLF J. P., Eur. Phys. J. D **4** (1998), 231.
[5] BORN M., WOLF E., *Principles of Optics*, Pergamon, Oxford 1975.
[6] STRATTON J. D., *Electromagnetic Theory*, McGraw-Hill Book. Co., Inc., New York, London 1941.
[7] KOLWAS K., DEMIANIUK S., KOLWAS M., J. Phys. B **29** (1996), 4762.
[8] VAN DE HULST H. C., *Light Scattering by Small Particles*, Chapman and Hall, New York 1957.
[9] MARKOWICZ P., KOLWAS K., KOLWAS M., Phys. Lett. A **236** (1997), 543.
[10] DE HEER W. A., SELBY K., KRESIN V., MASUI J., VOLLMER M., CHÂTELAND A., KNIGHT W. D., Phys. Rev. Lett. **97** (1987), 1805.
[11] SELBY K., VOLLMER M., MASUI J., KRESIN V., DE HEER W. A., CHÂTELAND A., KNIGHT W. D., Phys. Rev. B **40** (1989), 5417.
[12] SELBY K., KRESIN V., MASUI J., VOLLMER M., DE HEER W. A., SCHEIDEMANN A., KNIGHT W. D., Phys. Rev. B **43** (1991), 4565.
[13] BRÉCHIGNAC C., CAHUZAC PH., KABAÏLI N., LEYNIER J., SARFATI A., Phys. Rev. Lett. **68** (1992), 3916.
[14] BRÉCHIGNAC C., CAHUZAC PH., Phys. Rev. Lett. **70** (1993), 2036.
[15] DUTHLER C. J., JOHNSON S. E., BROIDA H. P., Phys. Rev. Lett. **26** (1971), 1236.
[16] HECHT J., J. Appl. Lett. **50** (1979), 7186.
[17] HECHT J., WEST W. P., BROIDA H. P., J. Chem. Phys. **71** (1979), 3132.
[18] HECHT J., Phys. Rev. B **40** (1989), 9982.
[19] EVERSOLE J. D., BROIDA H. P., Phys. Rev. B **15** (1977), 1644.
[20] KOLWAS K., KOLWAS M., ZALICKI P., Phys. Lett. A **167** (1992), 272.
[21] KOLWAS K., KOLWAS M., JAKUBCZYK D., Appl. Phys. B **60** (1995), 173.
[22] JAKUBCZYK D., KOLWAS M., KOLWAS K., J. Phys. B **30** (1997), 5567.
[23] SYNOWIEC M., KOLWAS K., KOLWAS M., Z. Phys. D. **40** (1997), 271.
[24] DEMIANIUK S., Doctor's Thesis (in Polish), Institute of Physics, Polish Academy of Sciences, 1999.
[25] KOLWAS K., DEMIANIUK S., KOLWAS M., Appl. Phys. B **65** (1997), 63.
[26] KOLWAS K., Appl. Phys. B **66** (1980), 467.
[27] BORGGREEN J., CHOWDHURY P., KEBAÏLI N., LUNDSBERG-NIELSEN L., LÜTZENKIRCHEN K., NIELSEN M. B., PEDERSEN J., RASMUSSEN H. D., Phys. Rev. B **48** (1993), 17507.
[28] MEIBOM P., ØSTEGÅRD M., BORGGREEN J., BJØRNHOLM S., RASMUSSEN H. D., Z. Phys. D **40** (1997), 258.
[29] REINERS T., ELLERT CH., SCHIDT M., HABERLAND H., Phys. Rev. Lett. **74** (1995), 1558.

Received September 15, 1999